

Thermodynamic properties of an interacting hard-sphere Bose gas in a trap using the static fluctuation approximation

Saleem I. Qashou

Department of Physics, Faculty of Science, University of Jordan, Amman, JORDAN

Mohamed K. Al-Sugheir

Department of Physics, The Hashemite University, Zarqa, JORDAN

Asaad R. Sakhel

Faculty of Engineering Technology, Al-Balqa Applied University Amman 11134, JORDAN

Humam B. Ghassib

Department of Physics, University of Jordan, Amman, JORDAN

A hard-sphere (HS) Bose gas in a trap is investigated at finite temperatures in the weakly-interacting regime and its thermodynamic properties are evaluated using the static fluctuation approximation (SFA). The energies are calculated with a second-quantized many-body Hamiltonian and a harmonic oscillator wave function. The specific heat capacity, internal energy, pressure, entropy and the Bose-Einstein (BE) occupation number of the system are determined as functions of temperature and for various values of interaction strength and number of particles. It is found that the number of particles plays a more profound role in the determination of the thermodynamic properties of the system than the HS diameter characterizing the interaction, that the critical temperature drops with the increase of the repulsion between the bosons, and that the fluctuations in the energy are much smaller than the energy itself in the weakly-interacting regime.

Keywords:

1. Introduction

The thermodynamic properties of a trapped interacting Bose gas have been investigated extensively in the last decade ^{1; 2; 3; 4; 5; 6}, ever since Bose-Einstein condensation (BEC) was realized for the first time in a trap in 1995 ⁷. Finite-size effects ⁸ and the possibility of BEC in one and two dimensions ⁹ have been explored. Numerical ⁵ studies of interacting BECs in traps as well as quasi one- and two-dimensional condensate expansion ¹⁰ due to the interactions have been carried out. In particular, the effect of the interaction on the transition temperature T_c ^{11; 12; 1} has been probed extensively. Further, the noninteracting trapped Bose gas has been a fascinating research topic ^{13; 14; 15; 4; 16} and its thermodynamic properties such as the BE occupation function, specific heat capacity, internal energy, and entropy have been calculated. A basic issue in this context is the role of the en-

ergy fluctuations. For example, Giorgini¹⁷ found that, below T_c , these fluctuations cause a shift in the excitation frequencies of order of a few percent.

The aim of this paper is to undertake a full investigation of the thermodynamic properties for a trapped hard-sphere (HS) Bose gas with small and large numbers of particles by using a discrete-states approach. The role of the energy fluctuations in determining these properties will be underlined.

We use the static fluctuation approximation (SFA)^{18; 19; 20} which includes in a relatively simple manner the above energy fluctuations. The principal feature of SFA is the replacement of the square of the local energy fluctuation operator $(\Delta\hat{E})^2$ with its mean value $\langle(\Delta\hat{E})^2\rangle$. $[\langle(\Delta\hat{E})^2\rangle]^{1/2}$ turns out to be much less than the chemical potential μ which, according to Giorgini¹⁷, places the fluctuations in our system in the collective-mode category. SFA has been used to study liquid ^4He ²¹, liquid ^3He ²², spin-polarized atomic hydrogen¹⁸, spin-polarized $^3\text{He-He II}$ mixtures¹⁹, ferroelectrics²⁰, and nuclear matter²³. All these are homogeneous systems. In contrast, SFA is used here for the first time to investigate an inhomogeneous-density system: a trapped Bose gas whose inhomogeneity is a result of external trapping. The non-uniform Bose condensed gas has been investigated by Öhberg and Stenholm⁵ in the framework of a Hartree-Fock (HF) formulation. However, HF theory fails at temperatures near the critical temperature T_c , whereas SFA works well below T_c . Hence our present SFA formulation of the trapped Bose gas may be regarded as a complementary method to that of Öhberg and Stenholm. Further, an approach is invoked according to which the particles are distributed in discrete energy levels; whereas most previous work, e.g.^{8; 4; 24; 25}, used a continuous density of states.

We find that thermal fluctuations, for the ground state of a BEC in a harmonic trap, reach a maximum at the BEC transition temperature, and decline afterwards as the temperature T rises. In addition, we find that at $g < 1 \times 10^{-3}$ the energy fluctuations are very small $\sim O(10^{-5})$ and do not influence the thermodynamic properties very much. The entropy is found to increase with T up to T_c , beyond which it begins to stabilize, reaching a plateau at higher T . Hence, the highest order in the system occurs when $T \rightarrow 0$; whereas at higher T disorder is independent of T . It turns out that the critical temperature for the onset of BEC decreases with the increase of the repulsion between the bosons. It is further found that a change in the number of particles of the system has quite a strong influence on the thermodynamic properties. The Bose-Einstein (BE) occupation function is studied as a function of T and the effect of interaction on the distribution of the bosons in different HO states is investigated. We find that indeed a large number of discrete HO states is needed ($\gg 100$) to describe strongly-repulsive BECs.

The paper is organized as follows. In Sec.2 the method is presented briefly. In Sec. 3 the performance of an updated version of the SFA code is analyzed. In Sec. 4 our results are discussed and compared to previous literature. In Sec. 5 our conclusions are listed. Appendix A.1 explains the SFA iterative procedure used, and Appendix A.2 describes the SFA method.

2. Method

We consider an interacting hard-sphere (HS) Bose gas of N particles in an isotropic, spherically symmetric, harmonic trap of trapping frequency $\omega_{ho} = 2\pi \times 10$ Hz and at finite temperature T . The strength of the interatomic interaction is characterized by the s-wave scattering length a_s , which is equivalent to the HS boson diameter in the low-energy and long-wavelength approximation. We consider a hard core repulsive interaction between the bosons. In what follows, we present only the key points of the method; details are relegated to Appendices A.1 and A.2.

2.1. SFA

Here we shed light on the small parameter of our approximation. As stated in the Introduction, we replace the square of the local energy fluctuation operator $(\Delta\hat{E}_m)^2$ for each state m with its mean value $\langle(\Delta\hat{E}_m)^2\rangle$. The energy fluctuation $\Delta\hat{E}_m$ is given by

$$\Delta\hat{E}_m = \hat{E}_m - \langle\hat{E}_m\rangle, \quad (1)$$

where \hat{E}_m is the energy operator of state m [Eq.(A.11)], and $\langle\hat{E}_m\rangle$ is the average value [Eq.(10)]. We define the small parameter of the approximation, written $\varphi_F(m, T)$, which appears in the thermodynamic functions in Sec.2.5 below, as

$$\varphi_F^2(m, T) = \langle(\Delta\hat{E}_m)^2\rangle. \quad (2)$$

That is,

$$\langle(\Delta\hat{E}_m)^2\rangle = \langle\hat{E}_m^2\rangle - \langle\hat{E}_m\rangle^2, \quad (3)$$

as usual. Essentially, $\varphi_F(m, T)$ is proportional to the magnitude of the interaction constant g as well as the average correlations between pairs of number fluctuations [see Eq.(A.4) below].

2.2. Hamiltonian

To evaluate the energy of the system, we use the following mean-field (MF) approach. We begin with the general form of the Hamiltonian:

$$\hat{H} = \int d\mathbf{r} \hat{\psi}^\dagger(\mathbf{r}) \left[-\frac{\hbar^2}{2m} \nabla^2 + V_{ext}(\mathbf{r}) \right] \hat{\psi}(\mathbf{r}) + \frac{1}{2} \int d\mathbf{r} \hat{\psi}^\dagger(\mathbf{r}) \hat{\psi}^\dagger(\mathbf{r}) V_{int}(\mathbf{r} - \mathbf{r}') \hat{\psi}(\mathbf{r}) \hat{\psi}(\mathbf{r}). \quad (4)$$

To describe the interaction between the bosons in the trap, we first consider a two-body HS contact potential given by

$$V_{int}(\mathbf{r}_1 - \mathbf{r}_2) = g\delta(\mathbf{r}_1 - \mathbf{r}_2), \quad (5)$$

where $g \equiv 4\pi\hbar^2 a_s/u$ is the interaction parameter, with a_s the s-wave scattering length in the low-energy and long-wavelength approximation and u the reduced bosonic mass. We further write the field operators as linear combinations of creation and annihilation operators:

$$\hat{\psi}(\mathbf{r}) = \sum_m \phi_m(\mathbf{r}) \hat{b}_m, \quad (6)$$

$\phi_n(\mathbf{r})$ being single-particle noninteracting wavefunctions for a particle at position \mathbf{r} and \hat{b}_m is the boson annihilation operator.

Substituting (5) and (6) into (4) and taking for $\phi_n(\mathbf{r})$ the harmonic oscillator wavefunctions in Cartesian coordinates:

$$\phi_m(\mathbf{r}) = \phi_{m_x}(x)\phi_{m_y}(y)\phi_{m_z}(z), \quad (7)$$

with

$$\phi_m(x) = \frac{1}{2^m m! \sqrt{\pi}} \exp(-x^2/2) H_m(x), \quad (8)$$

where $H_m(x)$ is the Hermite function of order m (and similarly for y and z), one gets for the second-quantized Hamiltonian for N interacting bosons in a harmonic trap

$$\begin{aligned} \hat{H} = & \sum_m \hbar\omega_{ho}(m + 3/2) \hat{b}_m^\dagger \hat{b}_m + \\ & \frac{g}{2} \sum_{c_1 c_2 c_3 c_4} \hat{b}_{c_1}^\dagger \hat{b}_{c_2}^\dagger \hat{b}_{c_3} \hat{b}_{c_4} \int \phi_{c_1}^*(\mathbf{r}) \phi_{c_2}^*(\mathbf{r}) \phi_{c_3}(\mathbf{r}) \phi_{c_4}(\mathbf{r}) d\mathbf{r}, \end{aligned} \quad (9)$$

m and c_i being integers representing harmonic oscillator (HO) states. Then, as shown in Appendix A.2 [from Eq.(A.7) to (A.12)], the MF average energy per state m can be written:

$$\langle \hat{E}_m \rangle = \hbar\omega_{ho}(m + 3/2) + \frac{1}{2}g \sum_{n=0}^{\infty} c(n, m) \langle \hat{n}_k \rangle, \quad (10)$$

where $\langle \hat{n}_k \rangle$ is the BE occupation function:

$$\langle \hat{n}_k \rangle = \frac{d_k}{\exp[(E_k - \mu)\beta] - 1}, \quad (11)$$

with $\beta \equiv 1/k_B T$, k_B being Boltzmann's constant, d_k a statistical weight defined by the degeneracy of the system, and $c(k, m)$ the elements of the interaction matrix obtained from the integral in Eq.(9):

$$c(n, m) = \frac{1}{d_m} \sum_{\substack{n_x, n_y, n_z \\ m_x, m_y, m_z}} \prod_{i=1}^3 \left[B_{n_i, m_i} \int_{-\infty}^{+\infty} \exp(-2u_i^2) H_{n_i}^2(u_i) H_{m_i}^2(u_i) du_i \right] \quad (12)$$

Here m must fulfill the condition $m = m_x + m_y + m_z$, which leads to a degeneracy in each state, and $d_m \equiv (m+1)(m+2)/2$ is the degeneracy of state m : $m_1 = m_x$, $m_2 = m_y$, $m_3 = m_z$, and similarly for n ; $u_1 = x$, $u_2 = y$, $u_3 = z$. The reason $c(n, m)$ has been divided by the degeneracy d_m is that Eq. (12) is a sum over all possible sets of degenerate HO states (m_x, m_y, m_z) satisfying $m = m_x + m_y + m_z$ and interacting with all possible sets of degenerate states (n_x, n_y, n_z) with $n = n_x + n_y + n_z$. However, Eq. (10) describes a particle in a given state m for a single set (m_x, m_y, m_z) interacting with all the other sets (n_x, n_y, n_z) . Therefore, to ensure correct counting, $c(n, m)$ must be divided by d_m . B_{n_i, m_i} stands for the normalization factor for each direction i , and is given by

$$B_{n_i, m_i} = \frac{1}{2^{n_i+m_i} n_i! m_i! \pi}. \quad (13)$$

Our computational limitations have restricted the rank of the matrix $c(n, m)$, i.e., the maximum values of n and m .

We use trap units for the energy and length, $\hbar\omega_{ho}$ and $a_{ho} = \sqrt{\hbar/m\omega_{ho}}$, respectively. Therefore,

$$g \rightarrow \frac{g}{\hbar\omega_{ho}} = 4\pi a_s a_{ho}^2; \quad (14)$$

and similarly $E \rightarrow E/\hbar\omega_{ho}$; by multiplying g by a factor a_{ho}^{-3} arising from the triple integral of the interaction matrix, g becomes $4\pi a_s$ in trap units ($a_s/a_{ho} \rightarrow a_s$).

2.3. Numerics

The integrals in Eq. (12) are determined by applying a standard Gaussian quadrature technique²⁶. The Hermite functions are evaluated by using the recursion formula²⁷

$$H_{n+1}(x) = 2xH_n(x) - 2nH_{n-1}(x); \quad (15)$$

with $H_0(x) = 1$ and $H_1(x) = 2x$, one can iterate the above formula to get $H_n(x)$ for any n .

2.4. Chemical potential

In what follows a new, simple technique is presented that facilitates a speedy and accurate evaluation of the chemical potential μ for each temperature T . Since the sum of $\langle \hat{n}_k \rangle$ [Eq.(11)] for a given μ yields the total number of particles, we define the function

$$f(\mu, T) = \left\{ N - \sum_{m=0}^M \frac{d_m}{\exp[(\langle E_m \rangle - \mu)\beta] - 1} \right\}^2, \quad (16)$$

which has been minimized at each T so as to tune $\mu(T)$ to a desired number of particles N by using Powell's minimization routine²⁶. Here M is the total number

of states used. However, for the evaluation of μ in SFA, the ‘corrected’ occupation function $\eta_0(m, T)$ weighted by d_m , which contains the fluctuations φ_F [Eq. (A.21)], has been used instead of $\langle \hat{n}_m \rangle$ [Eq. (11)]. The evaluation of φ_F using the SFA iterative procedure is explained in Appendix A.1.

Thus, one first evaluates μ for the noninteracting system by setting $\langle E_m \rangle = \hbar\omega_{ho}(m + 3/2)$ in Eq. (16); next this μ is used in the evaluation of $\langle E_m \rangle$ for an interacting system via Eq. (10). The energy of this interacting system is then fed back into Eq. (16) to get μ for the interacting system. This technique is somewhat similar to that used by Napolitano *et al.*¹⁵. M is tuned further to get the correct value for the specific heat capacity in the classical limit (Sec. 4.6.3).

2.5. Thermodynamic functions

In this section the equations used in the SFA program are reviewed briefly. The pressure is evaluated in trap units using

$$P\Omega = \frac{k_B T}{\hbar\omega_{ho}} \ln Q, \quad (17)$$

where Ω is the volume of the system, Q is the Gibbs partition function, and

$$\ln Q = - \sum_{m=0}^M q_0(m, T), \quad (18)$$

$q_0(m, T)$ being a discrete function given by Eq.(A.37).

According to Rochin²⁸, the “volume” Ω in the case of a non-uniform trapped Bose gas system can be written $\Omega = \omega_{ho}^{-D}$, where D is the dimensionality of the system (in our case $D = 3$), and ω_{ho} the trapping frequency. Further, we note that instead of evaluating P only, we have actually evaluated the ‘pressure’ as $P \times \Omega$ which has units of energy. Thus, even if P does not have the units of force per unit area, just as Ω does not have the units of volume, the most important fact is that $P \times \Omega$ has units of energy. In addition, we show in Appendix A.3 that our Eq.(18) yields the thermodynamic potential for a non-uniform trapped Bose gas system in the limit of an infinite number of states and very small fluctuations.

The internal energy is given by

$$U = - \left[\frac{\partial \ln Q}{\partial \beta} \right]_{\mu, \varphi_F, E} = \sum_{m=0}^M \left[\frac{\partial q_0(m, T)}{\partial \beta} \right]_{\mu, \varphi_F, E}, \quad (19)$$

where the derivative (19) has been calculated at constant μ , φ_F , and E . Otherwise, if we included the derivatives of μ , φ_F , and E with respect to β , we find that a physical behavior for the thermodynamic properties is not obtainable.

The specific heat is evaluated using

$$C_v = \left(\frac{\partial U}{\partial T} \right)_N = \frac{\partial}{\partial T} \sum_{m=0}^M \frac{\partial q_0(m, T)}{\partial \beta}. \quad (20)$$

Finally, the entropy is given by

$$S = \frac{U + P\Omega - \mu N}{T}. \quad (21)$$

In evaluating S , we find that μN contributes only a small amount to S and can therefore be ignored.

The thermodynamic equations (17) and (21) in our paper were previously used for nonuniform gases by Sevincli and Tanatar²⁴ but in different units than ours. Further, Grether *et al.*⁶ used Eq.(17) and Rochin²⁸ used (21) for nonuniform Bose gases.

3. Analysis of the performance of the SFA code

In what follows, a brief analysis of the performance of a more advanced version of the SFA program than that used in^{21; 22; 23} is presented. This version has been written in the C programming language and new features have been included that have enabled us to obtain $\mu(T)$ as in Sec.2.4, as well as $\varphi_F(m, T)$, and perform a convergence check of the iteration procedure.

3.1. Determining the Chemical Potential

Figure 1 shows μ as a function of $T/T_c^{(o)}$ for various g , where $T_c^{(o)} = 4.5113$ nK has been chosen as our reference temperature. These values of $\mu(T)$ have been obtained by the technique of Sec.2.4 using $\eta_0(m, T)$. $T_c^{(o)}$ has been evaluated from the noninteracting result²⁹:

$$T_c^{(o)} \sim 0.94 \frac{\hbar\omega_{ho}}{k_B} N^{1/3}, \quad (22)$$

for $N = 1000$ and $\omega_{ho} = 2\pi \times 10$ Hz; this value is used throughout the rest of the paper. Below the critical temperature, μ is – as expected – equal to the ground-state energy of the harmonic oscillator in the weakly-interacting regime, namely, ~ 1.5 in trap units. Above $T_c^{(o)}$, μ decreases steadily and acquires negative values. The chemical potential seems insensitive to the changes in the values of g indicated in the figure.

For comparison purposes, $\mu(T)$ is also displayed for $g = 1 \times 10^{-4}$, as obtained by the MF technique in Sec. 2.4 using $\langle \hat{n}_k(T) \rangle$. SFA and MF results shown are identical. The fact that μ below $T_c^{(o)}$ (~ 1.5) is close to the ground-state energy indicates that most of the particles reside in the condensate at $T < T_c^{(o)}$. These results are in line with those of Öhberg and Stenholm⁵ and Ketterle and van Druten⁹ for the ideal Bose gas. However, when g is increased to order 10^{-2} , μ below $T_c^{(o)}$ attains values higher than 1.5.

3.2. T-dependence of φ_F

Figure 2 displays the fluctuations $\varphi_F(m = 0, T)$ for the ground state ($m = 0$) of systems with $g = 1 \times 10^{-5}$, 2×10^{-5} , and 5×10^{-5} . The fluctuations increase with

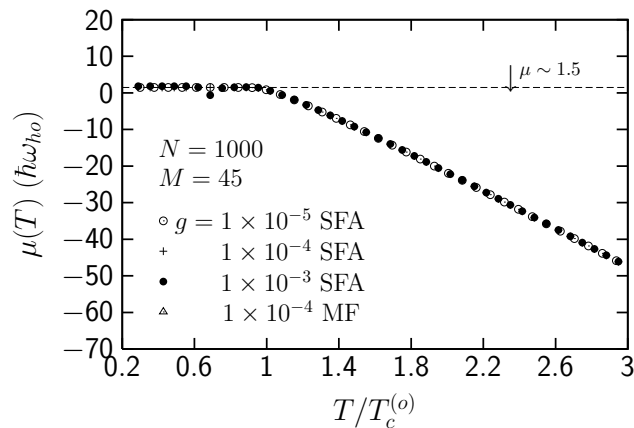


Fig. 1. The chemical potential μ for a trapped HS Bose gas of $N = 1000$ particles as a function of T for different g using SFA and MF techniques. The number of states is $M = 45$, and the trapping frequency is $\omega_{ho} = 2\pi \times 10$ Hz. The dashed line represents $\mu \sim 1.5$ and $T_c^{(o)}$ is the critical temperature for a noninteracting Bose gas.

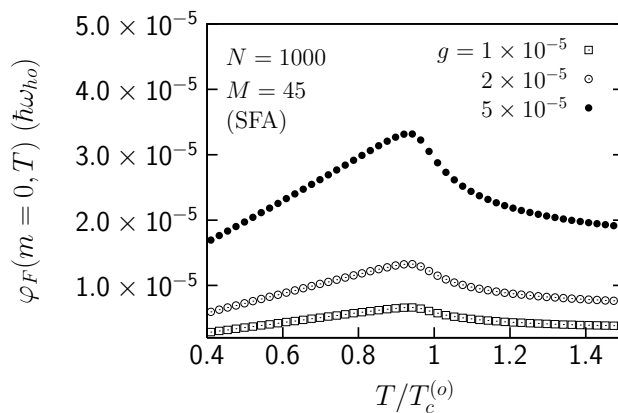


Fig. 2. SFA fluctuations in the energy $\varphi_F(m=0, T)$ as functions of T for a system of $N = 1000$ trapped HS bosons and $M = 45$ states at three interactions g . $T_c^{(o)}$ is the critical temperature for a noninteracting Bose gas.

T and show a maximum at the transition temperature T_c , beyond which they are damped. Note that T_c refers to the transition temperature in the *interacting* case; one can infer from Fig. 2 that $T_c < T_c^{(o)}$.

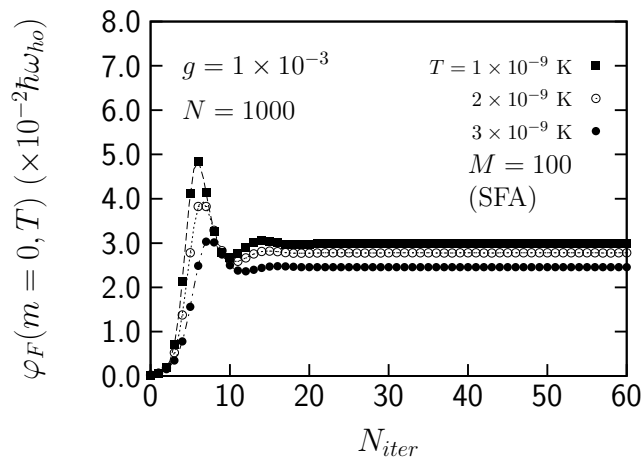


Fig. 3. SFA fluctuations $\varphi_F(m = 0, T)$ as functions of the number of iterations N_{iter} for the ground state of a trapped HS Bose gas of $N = 1000$ particles and $M = 100$ states at $g = 1 \times 10^{-3}$ and different T .

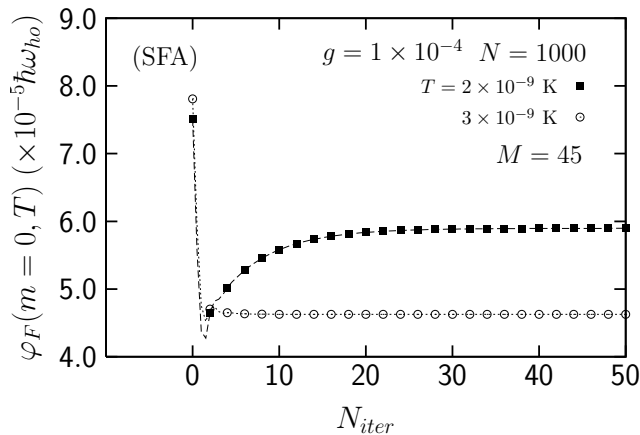


Fig. 4. SFA fluctuations $\varphi_F(m = 0, T)$ as functions of the number of iterations N_{iter} for the ground state of a trapped HS Bose gas of $N = 1000$ particles and $M = 45$ states at $g = 1 \times 10^{-4}$ and different T .

3.3. Convergence of SFA

To check the convergence of the iteration procedure outlined in Appendix A.1, $\varphi_F(m, T)$ is plotted versus the number of iterations N_{iter} in Figs. 3, 4, and 5 for several T and g . Figures 3 and 4, with $g = 1 \times 10^{-3}$ and 1×10^{-4} , respectively, show the need for a large number of iterations (~ 25) for SFA to converge to a steady

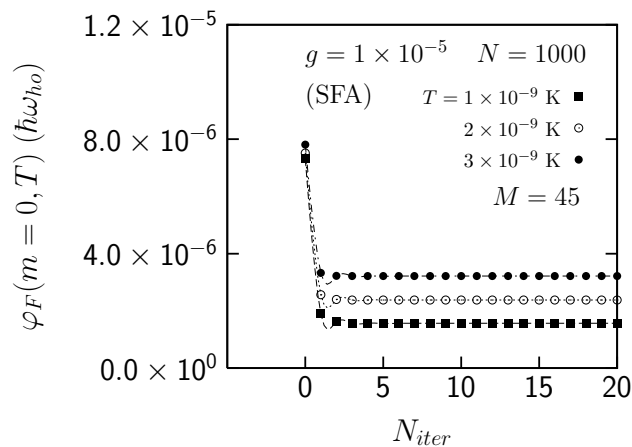


Fig. 5. SFA fluctuations $\varphi_F(m=0, T)$ as functions of the number of iterations N_{iter} for the ground state of a trapped HS Bose gas of $N = 1000$ particles and $M = 45$ states at $g = 1 \times 10^{-5}$ and different T .

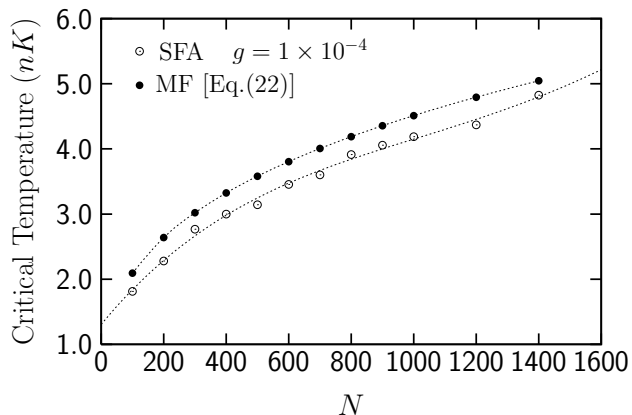


Fig. 6. Critical temperatures as functions of N for a HS Bose gas in a trap with $g = 1 \times 10^{-4}$ (T_c ; open circles) and for a noninteracting HS Bose gas ($T_c^{(o)}$; solid circles), evaluated within SFA and MF approaches, respectively.

value of $\varphi_F(m=0, T)$. In Fig. 5, with $g = 1 \times 10^{-5}$, on the other hand, $\varphi_F(m, T)$ converges rapidly after only 4 iterations for all the temperatures indicated. Thus, the higher the interaction, the larger the number of iterations needed to achieve convergence. It is, therefore, of the utmost importance to check the convergence of SFA calculations.

3.4. Critical temperature

Figure 6 shows a comparison between the critical temperature for an interacting (using SFA) and a noninteracting (using MF) system as a function of N . The solid circles pertain to $T_c^{(o)}$ of Eq. (22) for a noninteracting, and the open circles to T_c for an interacting, system with $g = 1 \times 10^{-4}$. The SFA results have been obtained from the peak positions of the specific heat capacities.

A considerable difference is noted between the two results, which shows that the critical temperature drops with increasing g . Further, the trend in T_c is almost the same as $T_c^{(o)}$. The critical temperature T_c obtained by SFA increases with N , as expected on physical grounds.

3.5. Failure of SFA at higher g

It is found that SFA breaks down at $g > 1 \times 10^{-3}$. The reason for this is that, at the higher interactions, the fluctuations become very large. As a result the exponent $\langle \hat{E}_m \rangle - \mu - \varphi_m$ becomes negative in

$$\eta_0(m, T) \equiv \frac{1}{2} \left\{ \frac{1}{\exp[\beta(\langle \hat{E}_m \rangle - \mu + \varphi_m)] - 1} + \frac{1}{\exp[\beta(\langle \hat{E}_m \rangle - \mu - \varphi_m)] - 1} \right\}. \quad (23)$$

This causes the second term on the right-hand side of $\eta_0(m, T)$ to acquire a negative sign as well. If a large number of states is negative, the sum of $\eta_0(m, T)$, weighted by the degeneracies d_m , may also turn out to be negative; whereas it is supposed to yield the total number of particles for an optimal μ . Essentially this kills the calculation, since $f(\mu, T)$ [Eq.(16)] will be far away from the true minimum. We may call this the ‘sign problem’ in the SFA method.

4. Results and Discussion

In this section the interrelationship between N , M , and g , the energy as a function of T , the occupancy of states, and the thermodynamic properties are presented.

4.1. Interrelationship between N , M , and g

Figure 7 displays the dependence of N on M for two values of g . For each N , the value of M is adjusted to the classical limit of the specific heat capacity, $C_v = 3Nk_B$, in the weakly-interacting regime. One can see that, for a given g , an increase in N necessitates a rise in M ; although the rise in M is fairly small for each increment of N , namely 100. Generally speaking, then, one would not need an infinite number of states to accommodate numbers of particles of order 100. It is when one seeks systems with $N \sim 10^6$ that the number of states is expected to shoot up to very large values. It is further found that the change of M with N is independent of g in the weakly-interacting regime, and M is mainly determined by N .

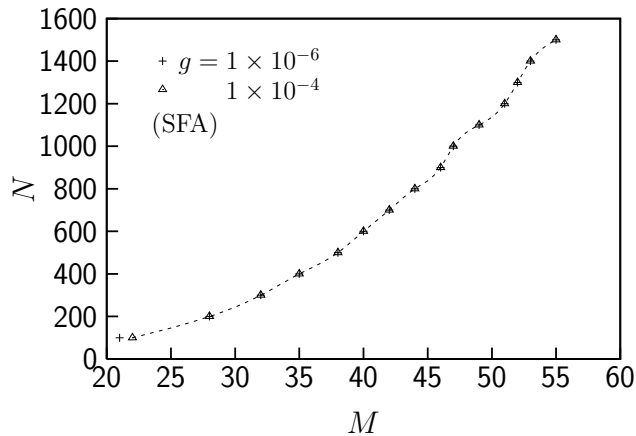


Fig. 7. Interrelationship between the number of particles N and the number of states M of trapped HS Bose gases at two values of g . The points (N, M) pertain to the classical limit $3Nk_B$ of the specific heat capacity.

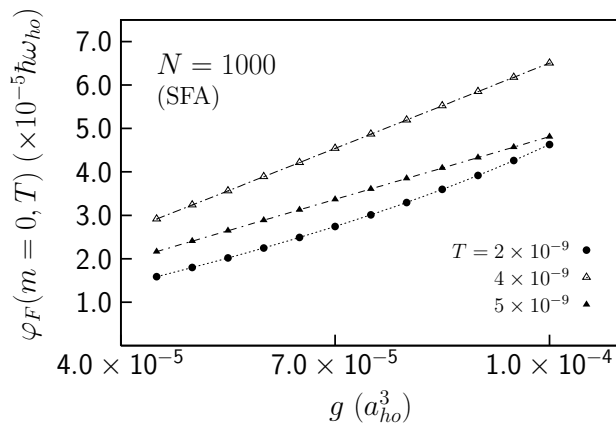


Fig. 8. SFA ground state fluctuation $\varphi_F(m=0, T)$ vs g at several T for $N = 1000$ particles.

4.2. Energy fluctuations

Figure 8 displays $\varphi_F(m=0, T)$ versus g for $N = 1000$ at various T . $\varphi_F(m=0, T)$ rises almost linearly as g is increased. Further, $\varphi_F(m=0, T)$ rises with T up to the transition temperature beyond which it drops.

4.3. Energy

Figure 9 displays the MF energy per particle $\langle \hat{E}_{m=0} \rangle / N$ in the condensate state, as obtained from Eq. (10), for $N = 1000$ particles and various g . The energy rises

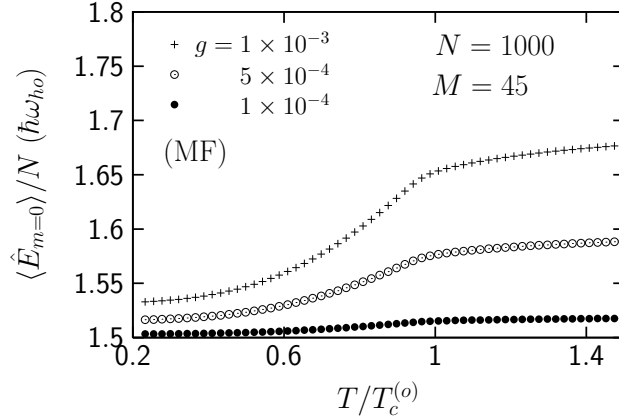


Fig. 9. The MF energy per particle for $m = 0$ as a function of T for $N = 1000$ trapped HS bosons, $M = 45$ states and three interaction parameters g .

initially at a faster rate below T_c than above it. As expected, the energy also rises with g . However, even though g and the changes in it are small, the variations in E vs T are relatively considerable; for example, at $T/T_c^{(o)} = 1.5$, one observes $\Delta E > 0.05$. This indicates that a small change in g causes $\langle \hat{n}_k(T) \rangle$ to attain a noticeably stronger T -dependence, i.e., $\langle \hat{n}_k(T) \rangle$ is very sensitive to variations in g . As the temperature rises, more particles are thermally excited out of the condensate to higher HO states. As a result, the energy arising from the interaction of the condensate with higher excited states increases with T , causing an increase in the total energy.

Figure 10 displays the behavior of $\langle \hat{E}_{m=0} \rangle / N$ when g is fixed and N is varied. Clearly, the energy rises with N ; as N increases, more particles occupy higher HO states. Notice that a relatively considerable change in N is required in order to increase E vs. T . For example, one needs $\Delta N = 300$ to get $\Delta E = 5 \times 10^{-3}$ at $T/T_c^{(o)} = 1.5$. This shows that a change in N has a weaker effect on the energy than a change in g .

4.4. Comparison to analytical results

The *total* mean-field energy of this work is

$$E_{total} = \sum_{m=0}^M \langle \hat{E}_m \rangle \langle \hat{n}_m \rangle, \quad (24)$$

where $\langle \hat{E}_m \rangle$ is given by Eq. (10). Figure 11 displays a comparison between the MF E_{total}/N (Eq. 24) for $N = 100$, $g = 1 \times 10^{-3}$, and $M = 100$, and the analytical E_{total}/N as obtained by Eqs.(47) and (67) of Su *et al.*³⁰ for the same parameters N and g . The two results almost match for $T < T_c^{(o)}$, and good agreement is obtained

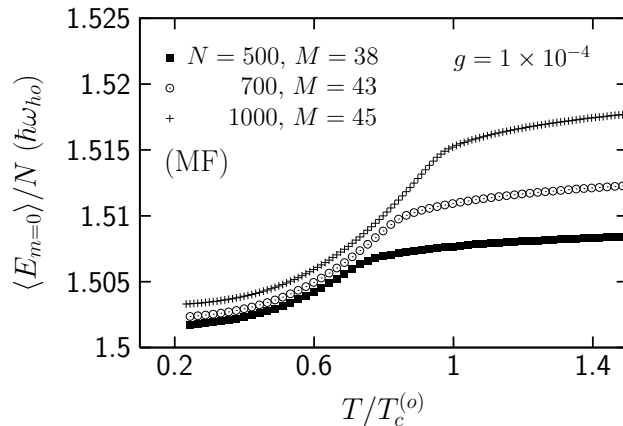


Fig. 10. The MF energy per particle for a fixed $g = 1 \times 10^{-4}$ and different M and N of a trapped HS Bose gas. In each case, M has been adjusted so as to attain a reasonable value for the classical limit of the specific heat capacity.

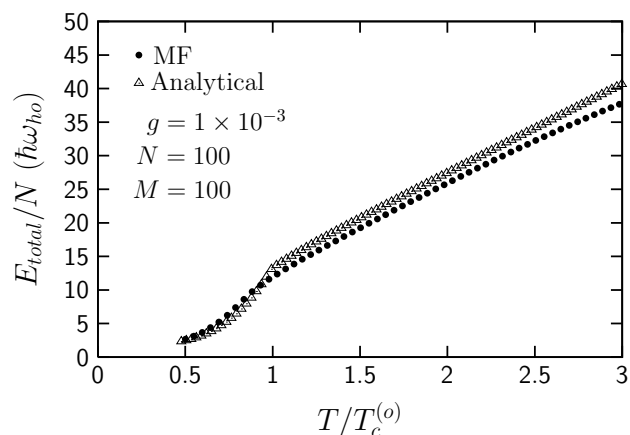


Fig. 11. The total MF energy per particle E_{total}/N for an interacting trapped HS Bose gas of $N = 100$ particles, $M = 100$ states, and $g = 1 \times 10^{-3}$. The open triangles show the analytical results by Su *et al.*³⁵ and the solid circles the MF results of the present work.

for $T > T_c^{(o)}$. Figure 12 is the same as Fig. 11; but for $N = 1000$. Again, the two results almost match for $T < T_c^{(o)}$; but beyond that, the deviation from the analytical results is substantial, particularly above $T = 1.5T_c^{(o)}$. The reason for this large deviation goes back to the limited maximum number of states that we can use. Had we been able to apply $M > 100$, the MF result in Fig.12 would have approached the analytical result as M was increased since the excited particles

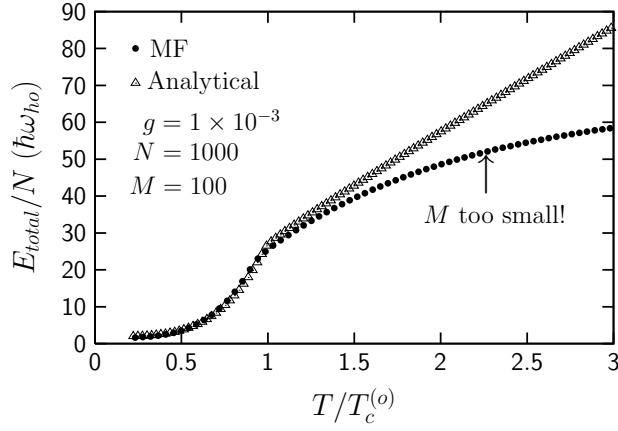


Fig. 12. The total MF energy per particle E_{total}/N for an interacting trapped HS Bose gas of $N = 1000$ particles, $M = 100$ states, and $g = 1 \times 10^{-3}$. The open triangles show the analytical results by Su *et al.*³⁵ and the solid circles the MF results of the present work.

would have been able to occupy higher states. In Fig. 11, the number of states was sufficient to accommodate all the excitations, and this is why there is good agreement above $T_c^{(o)}$. Further, the good agreement below $T_c^{(o)}$ arises from the fact that, at $T < T_c^{(o)}$, all particles are in the ($m = 0$) condensate state. Thus, there is no need for a large number of states to describe the system below $T_c^{(o)}$. In other words, the effect of excitations becomes significant only beyond $T = T_c^{(o)}$.

Thus, the MF model developed in Sec.2 works well. Likewise, the minimization technique of Sec.2.4 for evaluating the chemical potential is quite effective. A super-computer should enable one to reach states much higher than $M = 100$, particularly for the 3D case.

4.5. Occupancy of states

Figure 13 shows the fractional occupation number (condensate fraction) $\langle \hat{n}_0 \rangle / N$ versus T of bosons in the HO ground state, evaluated using SFA [crosses, $\eta_0(m = 0, T)$, Eq. (A.21)] and MF [open circles, $\langle \hat{n}_{k=0} \rangle$, Eq. (11)] for a system of $N = 1000$ particles, $M = 50$ states, and $g = 1 \times 10^{-4}$. The SFA $\eta_0(m = 0, T)$ is identical to the MF $\langle \hat{n}_{m=0}(T) \rangle$ because the fluctuations in the energy φ_F are much smaller than the energy itself at $g = 1 \times 10^{-4}$. One observes that, slightly above $T_c^{(o)}$, $\langle \hat{n}_0 \rangle / N$ drops to zero. In Fig. 14 we display for the same system the fractional occupation number for the first excited HO state $\langle \hat{n}_1 \rangle / N$ versus T . One can see that, while $\langle \hat{n}_0 \rangle / N$ decreases from 1 to almost zero at $T_c^{(o)}$, $\langle \hat{n}_1 \rangle / N$ increases steadily to a maximum at $T \approx 0.9T_c^{(o)}$ above which it drops systematically to zero. This kind of behavior has also been observed by Ketterle *et al.*⁹. Going further, we present in Fig. 15 $\langle \hat{n}_{50} \rangle / N$ for the same system. The occupation number in this rather high state keeps

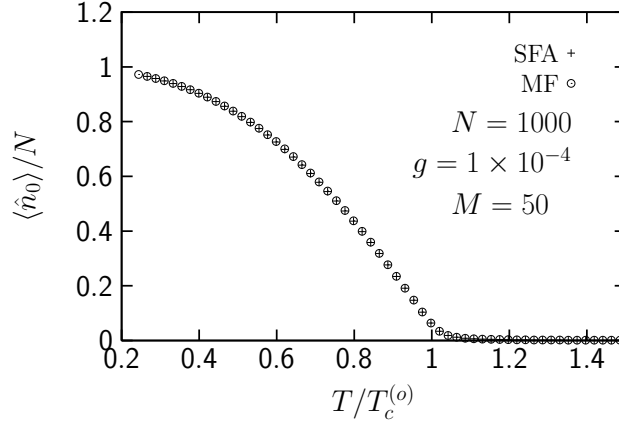


Fig. 13. SFA (crosses) and MF (open circles) fractional occupation numbers $\langle \hat{n}_0 \rangle / N$ as functions of T for the HO ground state, $m = 0$, of a system of $N = 1000$ trapped HS bosons, $M = 50$ states, with $g = 1 \times 10^{-4}$.

rising with T . If $M = 50$ had not been the highest state assigned in this particular calculation, $\langle \hat{n}_{50} \rangle$ would have reached a maximum beyond which it would have declined to zero, thus allowing other particles to be excited to states higher than $m = 50$ at higher T . Hence, in general, the maximum of $\langle \hat{n}_m \rangle$ is expected to shift to higher T as m becomes higher. It turns out, then, that M chiefly controls the overall distribution of N particles among the discrete states. It is to be emphasized that when one restricts M (to, e.g., 50), the BE occupation number at any given state m along with the chemical potential will be overestimated. This is because the bosons are shuffled back to lower states and are redistributed among them, particularly for $g > 0.01$. In this case, any states higher than $m = 50$ remain practically unoccupied.

Figure 14 shows that, when T reaches $T_c^{(0)}$, about 2.2% of the particles occupy the first excited state; and Fig.15 shows that only $\sim 0.5\%$ occupy the state $m = 50$. But as T rises further above $T_c^{(0)}$, the particles leave the condensate state $m = 0$ and occupy very high states such as $m = 50$; for example, at $T/T_c^{(0)} = 1.8$ we see that $\langle \hat{n}_{50} \rangle / N \sim 0.02$, i.e., 2% of the particles occupy our highest state. Nevertheless, for the values of g used in this investigation ($g \leq 1 \times 10^{-3}$), $M = 50$ seems to be a reasonable value, since $\langle \hat{n}_{50} \rangle / N$ is only 2% in Fig. 15.

Further, the maximum values of N and g we are able to use, namely $N = 1000$ and $g = 1 \times 10^{-3}$, correspond to $Na_s = Ng/(4\pi) = 7.96 \times 10^{-2}$, which is much less than 1. Consequently, we are way below the Thomas-Fermi regime defined by $Na_s \gg 1$.

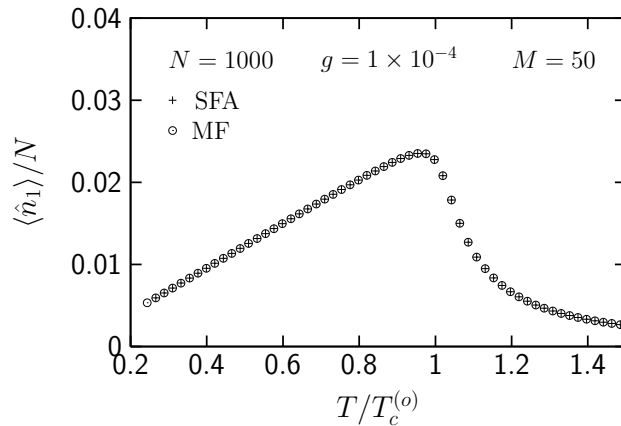


Fig. 14. SFA (crosses) and MF (open circles) fractional occupation numbers $\langle \hat{n}_1 \rangle / N$ as functions of T for the HO ground state, $m = 1$, of a system of $N = 1000$ trapped HS bosons, $M = 50$ states, with $g = 1 \times 10^{-4}$.

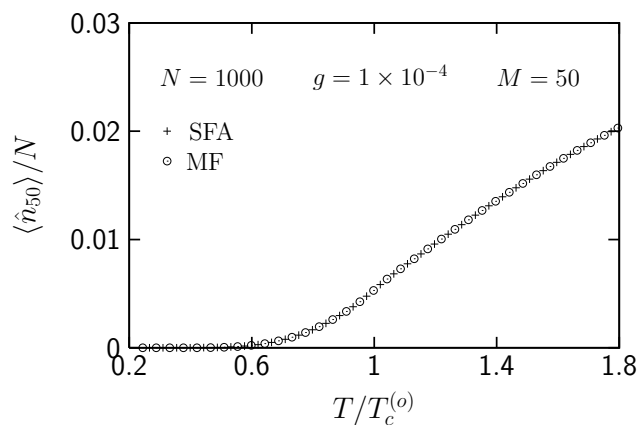


Fig. 15. SFA (crosses) and MF (open circles) fractional occupation numbers $\langle \hat{n}_{50} \rangle / N$ as functions of T for the HO ground state, $m = 50$, of a system of $N = 1000$ trapped HS bosons, $M = 50$ states, with $g = 1 \times 10^{-4}$.

4.6. Thermodynamic properties

4.6.1. Critical Temperature

Figure 16 displays $\langle \hat{n}_0 \rangle / N$ for a fixed $N = 1000$ particles and different g . T_c does not change appreciably between $g = 1 \times 10^{-4}$ and 1×10^{-3} ; but on increasing g to 0.05, T_c drops noticeably by $\sim -0.2T_c^{(o)}$ which is about 10 times the result of Giorgini *et al.*¹¹: $\Delta T \sim -0.016T_c^{(o)}$, the shift in $T_c^{(o)}$ being given by these authors

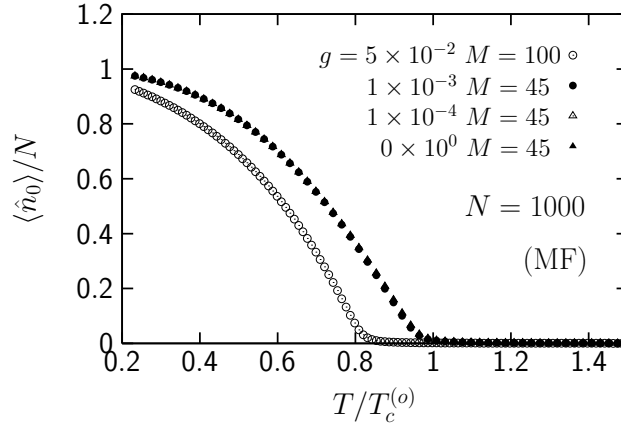


Fig. 16. The MF fractional occupation number $\langle \hat{n}_0 \rangle / N$ for $N = 1000$ trapped HS bosons and $M = 100$ states, for $g = 0.00$ (noninteracting system) and $g = 0.05$ (interacting system).

as

$$\frac{\delta T_c}{T_c^{(0)}} = -1.3 \frac{a}{a_{ho}} N^{1/6}. \quad (25)$$

Thus, there is a large discrepancy between the shift of T_c as obtained from our MF approach and that from Eq. (25). The reason for this large discrepancy is that, at higher interactions, the current HO wave function –originally designed for a weakly-interacting system– becomes inadequate for the description of a trapped Bose gas with $g = 0.05$. This is because the bosonic wave functions begin to broaden substantially away from their width described by $\exp(-x^2/2)$ in Eq.(8), and one should rather apply a parameterized Gaussian with a variable width described by $\exp(-\alpha x^2)$, where α is an adjustable parameter obtainable by variational techniques. We thus anticipate that, if an optimized wave function is used in our calculations, T_c will approach that of Giorgini *et al.*¹¹. We will investigate this issue in the future.

4.6.2. Internal energy

Figure 17 displays the internal energy per particle U/N as a function of T for different g , keeping $N = 1000$ fixed. U rises with T ; but it does not change appreciably with the variations in g . This indicates that the rate of two-body collisions is low in the weakly-interacting regime. The rise of U with T is partly due to the thermal expansion of the Bose gas towards the edges of the external trapping potential. As it approaches the edges of the trap, the gas gains more potential energy. Figure 18 shows the variations of $U(T)$ with N , g being kept fixed at 1×10^{-4} . A change in N causes a much more pronounced change in the thermodynamic properties than a change in g within the displayed range. This is because, as N rises, the density

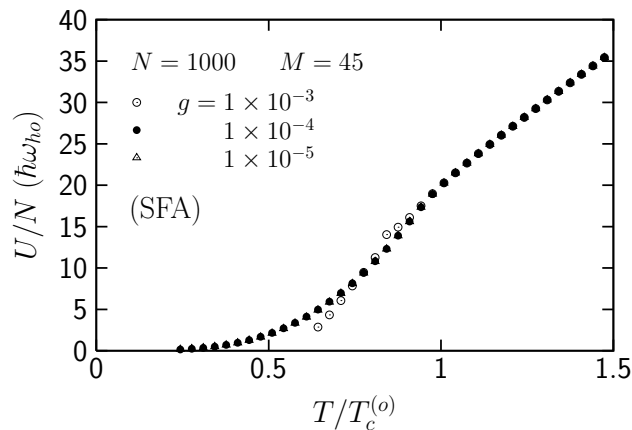


Fig. 17. The SFA internal energy per particle U/N as a function of T for $N = 1000$ trapped HS bosons, $M = 45$ states, and different g .

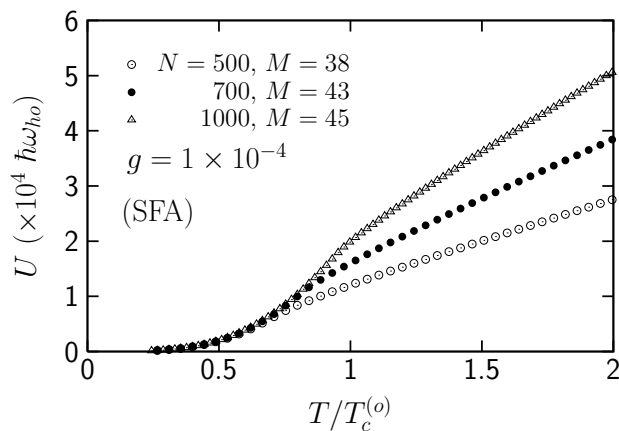


Fig. 18. The SFA internal energy per particle U/N as a function of T for a fixed $g = 1 \times 10^{-4}$, and different N and M of trapped HS Bose gases.

of the system rises, and therefore the rate of collisions increases, altering the thermodynamic properties substantially. In this case, $U(T)$ is initially insensitive to the changes in g and N at lower T up to $T \sim 0.75T_c^{(0)}$; but then towards $T = T_c^{(0)}$ the deviations in the behavior of $U(T)$ become noticeable at various N .

4.6.3. Specific heat

Figure 19 shows the specific heat capacity per particle C_v/N versus T in units of k_B for a system of $N = 1000$ bosons and different g . The behavior of $C_v =$

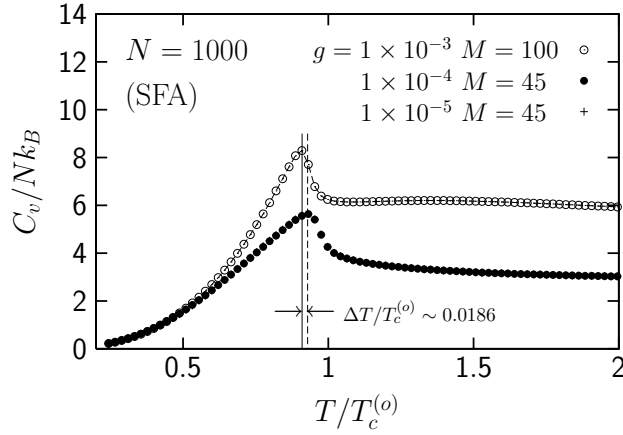


Fig. 19. The SFA specific heat capacity per particle C_v/N in units of k_B for $N = 1000$ trapped HS bosons for different g and M . The shift in the transition temperature is indicated.

$(\partial U/\partial T)_\Omega$ conforms with the behavior of U for the same systems in Fig. 17 at $g = 1 \times 10^{-5}$ and 1×10^{-4} . Initially, the slope of U increases with T up to T_c , after which it begins to decline and then stabilizes at higher T towards the classical regime. The appearance of a peak in C_v can also be directly attributed to the behavior of $\mu(T)$ in the neighborhood of T_c displayed in Fig. 1 since C_v given by Eq.(20) is connected to $\mu(T)$ via $q_0(m, T)$ [Eq.(A.37)]. Note that below T_c , $\partial\mu/\partial T \sim 0$, and when it approaches $T_c^{(o)}$, $\partial\mu/\partial T$ suddenly drops to a negative value (see Fig. 1). This abrupt change in $\mu(T)$ and $\partial\mu/\partial T$ causes a jump in $q_0(m, T)$ and $\partial q_0(m, T)/\partial T$ which explains the appearance of a peak in C_v . Alternatively, this ‘bump’ in C_v is clearly an ‘order-disorder’ transition since $C_v = T(\partial S/\partial T)_\Omega$. We note that C_v stabilizes at approximately the classical value of $\sim 3Nk_B$ ³¹ for $g = 1 \times 10^{-5}$ and 1×10^{-4} . However, for $g = 1 \times 10^{-3}$, a larger number of states $M = 100$ was taken to accommodate the need of particles to occupy higher HO states. This leads to a larger classical limit for C_v , namely, $6Nk_B$, as we are now approaching the strongly-interacting regime. In fact, it was found that, for large interactions $g \geq 1 \times 10^{-3}$, SFA calculations do not converge for $M < 100$. Figure 19 shows also that the signature of the transition –i.e., the peak of C_v – shifts to lower T by an amount $\Delta T/T_c^{(o)} \sim -0.0186$ as g rises from 1×10^{-4} to 1×10^{-3} . Using formula (25), we get for $\Delta T/T_c^{(o)}$ between $g = 4\pi a_c = 1 \times 10^{-3}$ and 1×10^{-4} the value $\Delta T/T_c^{(o)} \sim -2.944 \times 10^{-4}$ K which is two orders of magnitude smaller than our SFA result for ΔT .

Figure 20 shows C_v for a fixed g and various N . We observe that the amplitude of the peak in C_v rises with increasing N . Further, the peak shifts to higher T as N is increased, indicating that T_c increases. This is in line with the result for dilute Bose gases $T_c^{(0)} \sim 0.94(\hbar\omega_{ho}/k_B)N^{1/3}$ ²⁹.

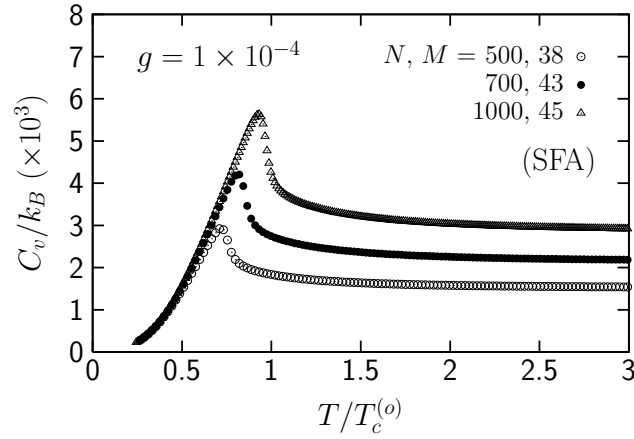


Fig. 20. The SFA specific heat capacity per particle C_v/N in units of k_B at a fixed $g = 1 \times 10^{-4}$ and different N and M of trapped HS Bose gases.

4.6.4. Entropy

Figure 21 displays the entropy per particle S/N in units of k_B versus T for different g at a fixed $N = 1000$. The entropy rises steeply below $T_c^{(0)}$, but then kinks over towards a plateau. Figure 22 is the same as Fig. 21, except that we keep g fixed at 1×10^{-4} and vary N . Thus, as for C_v , S eventually reaches the classical limit at higher T . Again the change in g from 1×10^{-5} to 1×10^{-3} does not have an appreciable effect on the thermodynamic properties. The entropy reveals higher order as $T \rightarrow 0$; in fact, as $T \rightarrow T_c^{(o)}$ the previously mentioned order-disorder transition is observed.

4.6.5. Pressure

Figure 23 displays the pressure $P(\times\Omega)$ as a function of T for the same systems of Fig. 21. P rises with T steeply up to $T_c^{(0)}$, after which it kinks slightly towards a lower slope. Figure 24 is the same as Fig. 23, but for fixed g and various N . We note that, at lower T up to $T/T_c^{(0)} \sim 0.75$, P is the same for all N ; but as one approaches $T_c^{(0)}$ the pressures for different N begin to deviate substantially from each other. At higher T , the slope of $P\Omega$ vs. T in Fig. 23, evaluated between $T/T_c^{(0)} = 1.0$ and 1.5 , is $\sim 2.305 \times 10^{12} \text{ K}^{-1}$. This value is very close to the classical value Nk_B divided by the trap energy unit $\hbar\omega_{ho}$, where $Nk_B/\hbar\omega_{ho} = 2.084 \times 10^{12} \text{ K}^{-1}$ for $\omega_{ho} = 2\pi \times 10$ Hz and $N = 1000$ particles. The same is true for Fig. 24, where the slope is different for each N in the classical limit.

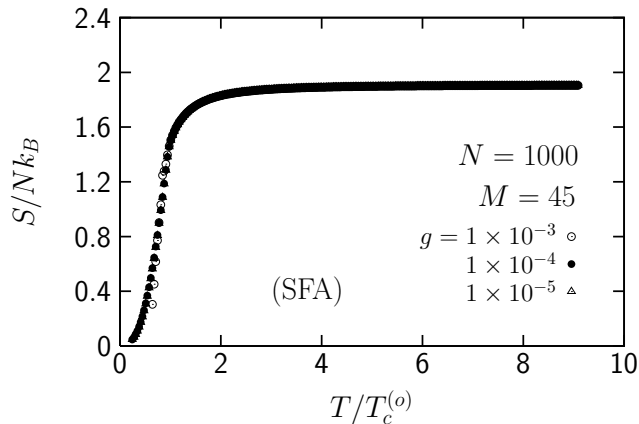


Fig. 21. The SFA entropy per particle S/N in units of k_B as a function of T for $N = 1000$ trapped HS bosons, $M = 45$ states, and different g .

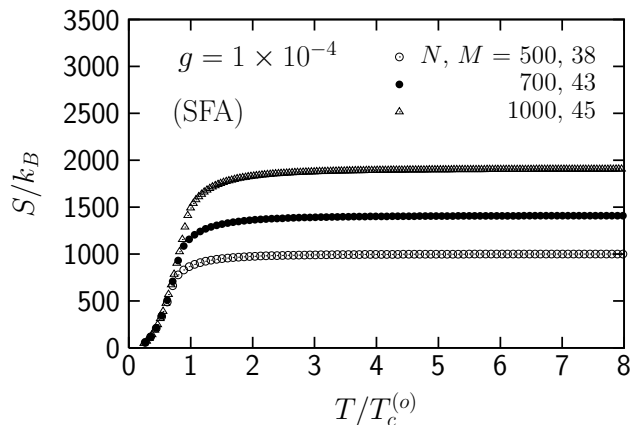


Fig. 22. The SFA entropy as a function of T in units of k_B for a fixed $g = 1 \times 10^{-4}$ and different N and M of trapped HS Bose gases.

4.7. Comparison to previous work

Öhberg and Stenholm⁵ presented qualitatively a numerical study of an inhomogeneous Bose gas by solving the Hartree-Fock equations for systems with repulsive interactions and restricting the number of particles, much as we do in our present study. They calculated the condensate density profiles and the thermally excited parts of the density as functions of temperature, particle number, and interaction strength and found that, above the critical temperature, there is no condensate. They further noted that HF theory does not describe the Bose gas well for all T

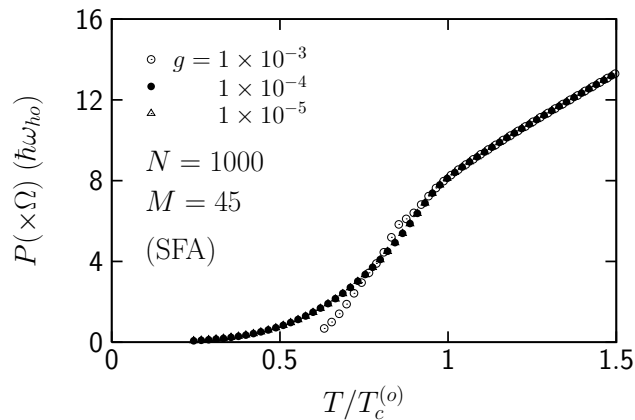


Fig. 23. The SFA pressure ($P \times \Omega$) as a function of T for $N = 1000$ trapped HS bosons, $M = 45$ states, and different g .

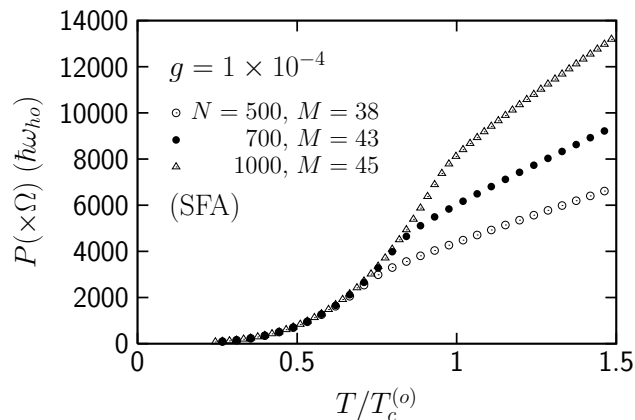


Fig. 24. The SFA pressure ($P \times \Omega$) as a function of T for a fixed $g = 1 \times 10^{-4}$ and different N and M of trapped HS Bose gases.

and that their theory breaks down near the critical temperature, contrary to SFA. In fact, we have shown that SFA functions well below T_c . The HF equations were solved by using an iterative approach which involves a density $n(\mathbf{r})$, then solving them for this density and using the new eigenfunctions to calculate a new density, and so on. This procedure was then iterated until one found a self-consistent solution for the density and eigenfunctions. The convergence of this method was checked by tracing the value of the ground-state energy. Thus, their main achievement was to obtain the density of the gas as a function of T . We note that, as we do, Öhberg and Stenholm used a limited number of states which they did not show

explicitly. In contrast to their approach, we used a fixed eigenfunction and obtained the thermodynamic properties by iterating the energy fluctuations [Eq. (A.33)].

Ketterle and van Druten⁹ investigated BECs in traps for a finite number of particles in an ideal Bose gas. They found that the signature of BECs, namely a discontinuity in the specific heat capacity for a small number of particles, is very similar to an infinite number of particles; that as one tightens the confinement, T_c rises; and that BEC is possible in 1D and 2D. Further, the population of the first excited state for $N \rightarrow \infty$ is negligible, even in the absence of interactions. As mentioned in Sec. 4.5, our occupation function $\langle \hat{n}_1 \rangle / N$ agrees with that shown by these authors in Fig.2 of their paper; but they did not display the occupation function for states higher than $m = 1$. In contrast, we have displayed the occupation function for $m = 50$ in Fig. 15.

Giorgini *et al.*¹¹ presented results for the temperature-dependence of the condensate fraction and the dependence of the critical temperature on the interaction between the bosons in a harmonic potential. They found that the thermal depletion of the condensate is enhanced in the presence of repulsive interactions, and that T_c shifts to lower values with increasing repulsive interactions. In addition, finite-size effects do affect the thermodynamic properties; however, interactions play a more profound role as they lead to significant depletion of the condensate. Further, when one increases the number of atoms, the interactions become more profound. Interestingly, comparing our figures displaying the thermodynamic properties for different N and fixed g to those for different g and fixed N , we arrive at the same conclusion. Finally, Giorgini *et al.* argued that the shift in the critical temperature is the combined effect of a finite number of particles plus the interactions. They found that the shift $\delta T_c^{(o)}$ arising from finite-size effects is always negative and vanishes at large N .

Kao and Jiang¹² provided a theoretical treatment for the effect of interactions on T_c . They noted that a finite number of particles usually drags a system away from the thermodynamic limit and that the effect of interactions is the hardest to treat among all other effects. This is substantiated by the present work since, as mentioned in Sec. 3.5, SFA breaks down at $g \geq 1 \times 10^{-3}$. In particular, they referred to the work of Giorgini *et al.*¹¹ and noted that these authors incorporated only thermal effects into their calculations of the shift of T_c and ignored the effect of the condensate component. Accordingly, Kao and Jiang considered this effect and underlined the importance of the interaction between the condensate atoms themselves, since even near the transition a small fraction of atoms resides in the condensate state at the trap center. Inspecting our Fig. 13, we also see that at T_c there is indeed a remaining small condensate fraction. The interaction between this remaining fraction and the thermal component is considered explicitly in our work. Further, they treated the system of condensate plus thermal component as a two-fluid model and showed that the energy gap between the thermal and condensate components determines the shift in the transition temperature.

Kao *et al.*¹³ studied ideal Bose gases trapped in a generic power-law potential,

using the grand canonical ensemble. Corrections to the thermodynamic properties due to a finite number of particles were evaluated, such as the transition temperature of the system as well as the condensate fraction. It was further argued that when the system has a finite number of particles, it is very important to consider the occupation fraction of excited states.

Napolitano *et al.*¹⁵ considered a finite number of noninteracting bosons trapped in a three-dimensional isotropic harmonic oscillator trap, and evaluated the corresponding heat capacity. For this purpose, they used the approach of Ketterle and van Druten⁹. In order to provide a signal for a phase transition – a discontinuous heat capacity – they calculated the heat capacity numerically for a fixed number of particles, C_N , which at the time their paper was published had not been measured. First, they evaluated $\mu(T)$ from the normalization condition

$$N = \sum_{n=0}^{\infty} \gamma_n \eta(E_n), \quad (26)$$

where $\eta(E_n)$ is the BE occupation function, $\gamma_n \equiv (n+1)(n+2)/2$ is the degeneracy of the HO state n , and $E_n \equiv n\hbar\omega_{ho}$ is the energy eigenvalue. For $T < T_c^0$, the ground state $n = 0$ of the system is macroscopically occupied. Once the chemical potential had been evaluated, the other thermodynamic properties followed easily. To obtain $\mu(T)$, they found the roots of the equation

$$S(\mu, T) \equiv \sum_{n=0}^Q \gamma_n \eta(E_n) - N, \quad (27)$$

for which $S(\mu, T) = 0$; a technique which bears some resemblance to ours in Sec. 2.4. In our case, we adjust the value of M (their Q) to give the correct classical limit of the specific heat capacity for noninteracting trapped Bose gases, namely, $3Nk_B$. However, in their approach, they ensured the convergence of $\mu(T)$ by iterating Eq.(27), with $S(\mu, T)$ set to 0, each time increasing the number of states Q , calculating the resulting $\mu(T)$ thereof, and comparing it to that for the previous values of Q . If the new $\mu(T)$ differed from the previous value by only a small increment, then this procedure was likely to have converged. Thus, they kept on increasing Q until convergence was achieved. Then they evaluated the specific heat capacity for several values of N and showed that there was a discontinuity in the thermodynamic limit; whereas the discontinuity vanished in systems with a finite number of particles. Our results for the specific heat capacity for finite systems in the weakly-interacting regime also reveal the absence of a discontinuity in C_v . In fact, the work of Napolitano *et al.* is one of the rare investigations of trapped Bose gases that use a discrete-states approach.

Grossmann and Holthaus⁴ looked into the BEC of relatively few particles in traps and considered particularly the effects of particle number on the condensation temperature and specific heat capacity. They evaluated the thermodynamic properties and found that the emergence of the λ -point in their specific heat capacity was solely due to the external trapping potential.

Gnanapragasam *et al.*¹⁶ calculated the occupation number of atoms in the ground state of an ideal Bose gas and an interacting Bose gas in a trap. From this, they investigated the effects of temperature and interaction on the condensate properties. They found that the depletion of the condensate rises with the rise in interaction and temperature, and that repulsive interactions stabilize the above systems; whereas in the case of attractive interactions, the systems up to certain negative g are stabilized by the zero-point repulsive energy arising from the confinement. We may argue that the signature for the stability of our systems is the convergence of SFA calculations to stable values of the fluctuations $\varphi_F(m, T)$ and the chemical potential $\mu(T)$. In any case, we did not have to worry about the stability issues of our systems. This is because the repulsive HS interactions between the bosons balance the compressional forces arising from the external trapping potential that try to squeeze the Bose gas radially towards the center of the trap. Further, we found similarly that as the temperature and interaction are increased, more and more particles are depleted out of the condensate. This result is in line with Gnanapragasam *et al.*¹⁶.

Grether *et al.*⁶ described the HO trapping of bosons and fermions in lower dimensions, the goal being to understand these structures. Further, they considered a d -dimensional noninteracting boson or fermion gas trapped by several mutually perpendicular harmonic oscillator potentials and showed that, in the thermodynamic limit, the specific heat capacity for a trapped Bose gas in 3D reaches $3Nk_B$. They found that BEC can only occur when $d + \delta > 2$, where d is the dimensionality of the system, and δ the number of HO potentials used that are mutually perpendicular to each other. In summary, the authors calculated the thermodynamic properties and densities for ideal Bose and Fermi gases trapped in δ mutually perpendicular trapping potentials. It turns out that the behavior of some thermodynamic properties obtained here by using SFA is quite similar to theirs (Fig.2 of their paper).

5. Conclusions

In summary, we have presented a formal investigation of the thermodynamic properties of a trapped, interacting HS Bose gas of finite size in the weakly-interacting regime, using the static fluctuation approximation (SFA). Our basic goal was to investigate the effect of energy fluctuations on these thermodynamic properties.

We find that these fluctuations are much smaller than the energy itself in the weakly-interacting ($g \leq 10^{-3}$), low-density regime. When the interactions are of order $g = 10^{-2}$, the energy fluctuations rise substantially and SFA breaks down in this highly-interacting regime.

Further, the critical temperature $T_c^{(0)}$ drops with increasing interactions for a fixed number of particles N , and rises with increasing N at fixed interaction strength.

In addition, changing g in the range from 0 to 1×10^{-3} does not have any

significant effect on the thermodynamic properties; but changing N while keeping g fixed has a more profound effect.

We have also found that the specific heat capacity for a fixed g increases with increasing N . The specific heat in the weakly-interacting regime, with a correctly adjusted total number of states, reaches the classical limit $3Nk_B$ at sufficiently high temperatures.

Appendix A.

A.1. Iterative procedure

Here we outline briefly the iterative method used to determine the energy fluctuations $\varphi_F(m, T)$ using SFA equations¹⁸, modified for a trapped HS Bose gas system. The basic point is to solve the nonlinear equations presented below, particularly Eq.(A.4), so as to obtain stable values for $\varphi_F(m, T)$. The procedure is constructed from a loop over all temperatures T , with chosen steps ΔT , and an inner loop, conducting iterations at each T to determine $\varphi_F(m, T)$. Hence, for each T :

- (1) one first assigns initial values for $\varphi_F(m, T)$ for all states m and the true correlations between the number fluctuations $\langle \Delta \hat{n}_m \Delta \hat{n}_k \rangle_c$ for $m \neq k$. Then an inner loop is started which conducts an iterative procedure to optimize the values of $\varphi_F(m, T)$ and $\langle \Delta \hat{n}_m \Delta \hat{n}_k \rangle_c$.
- (2) At the beginning of each iteration, the function $f(\mu, T)$ [Eq. (16)] is minimized with respect to the chemical potential $\mu(T)$ only.
- (3) Then having, determined $\mu(T)$ from the minimization, one evaluates the mean of the square of the number fluctuations:

$$\langle (\Delta \hat{n}_m)^2 \rangle = \eta_0(m, T)[1 + \eta_0(m, T)] + 2\eta_1(m, T) \frac{1}{2}g \sum_{k=1}^M c(m, k) \langle \Delta \hat{n}_k \Delta \hat{n}_m \rangle_c, \quad (\text{A.1})$$

where $\eta_1(m, T)$ is given by (A.21) below, and $c(m, k)$ is the interaction matrix, Eq. (12).

- (4) The correlations between the fluctuations are updated, using $\langle (\Delta \hat{n}_m)^2 \rangle$ in

$$\langle \Delta \hat{n}_m \Delta \hat{n}_k \rangle = \langle (\Delta \hat{n}_m)^2 \rangle \delta_{m k} + \langle \Delta \hat{n}_m \Delta \hat{n}_k \rangle_c. \quad (\text{A.2})$$

- (5) $\langle \Delta \hat{n}_m \Delta \hat{n}_k \rangle$ is used to update the true correlations between the fluctuations,

according to

$$\begin{aligned}
 \langle \Delta \hat{n}_m \Delta \hat{n}_k \rangle_c &= \eta_1(m, T) g \sum_{i=1}^M c(m, i) \langle \Delta \hat{n}_i \Delta \hat{n}_k \rangle \\
 &= \eta_1(m, T) g c(m, k) \langle (\Delta \hat{n}_k)^2 \rangle + \\
 &\eta_1(m, T) g \sum_{i=1}^M c(m, i) \langle \Delta \hat{n}_i \Delta \hat{n}_k \rangle_c.
 \end{aligned} \tag{A.3}$$

- (6) The fluctuations of the energy are calculated using the updated correlations $\langle \Delta \hat{n}_m \Delta \hat{n}_k \rangle_c$:

$$[\varphi_F(m, T)]^2 = \frac{g}{\eta_1(m, T)} \sum_{i=1}^M c(m, i) \langle \Delta \hat{n}_i \Delta \hat{n}_m \rangle_c \tag{A.4}$$

- (7) One goes back to step (2), using the updated $\varphi_F(m, T)$ and $\langle \Delta \hat{n}_m \Delta \hat{n}_k \rangle_c$, and steps (2)-(7) are repeated for a specified number of iterations.
 (8) At the end of the iterations, the procedure changes the temperature and is repeated.

A.2. SFA

In this appendix, we derive the thermodynamic properties using the static fluctuation approximation. We begin with the Heisenberg representation of the creation operator $\hat{b}_m^\dagger(\tau)$ given by

$$\hat{b}_m^\dagger(\tau) = \exp(\tau \hat{H}) \hat{b}_m^\dagger(0) \exp(-\tau \hat{H}). \tag{A.5}$$

This satisfies the equation of motion

$$\frac{d\hat{b}_m^\dagger}{d\tau} = [\hat{H}, \hat{b}_m^\dagger(\tau)] = \hat{E}_m \hat{b}_m^\dagger(\tau). \tag{A.6}$$

If we decompose the Hamiltonian \hat{H} in (9) into a noninteracting and interacting part, \hat{H}_0 and \hat{H}_{int} , respectively, where \hat{H}_0 is the first, and \hat{H}_{int} the second term on the right-hand-side of Eq.(9), then \hat{H}_0 commutes with \hat{b}_m^\dagger according to

$$[\hat{H}_0, \hat{b}_m^\dagger] = \hbar\omega_{ho}(m + 3/2) \hat{b}_m^\dagger; \tag{A.7}$$

for the interacting part, we get

$$[\hat{H}_{int}, \hat{b}_m^\dagger] = \frac{1}{2}g \sum_{n_1 n_2 n_3} c(n_1, n_2, n_3, m) \hat{b}_{n_1}^\dagger \hat{b}_{n_2}^\dagger \hat{b}_{n_3}, \tag{A.8}$$

where

$$c(n_1, n_2, n_3, m) = \int d\mathbf{r} \phi_{n_1}^*(\mathbf{r}) \phi_{n_2}^*(\mathbf{r}) \phi_{n_3}(\mathbf{r}) \phi_m(\mathbf{r}). \tag{A.9}$$

The energy \hat{E}_m can then be evaluated from the commutation relation

$$[\hat{b}_m, [\hat{H}, \hat{b}_m^\dagger]] = \hat{E}_m. \quad (\text{A.10})$$

which leads to

$$\hat{E}_m = \hbar\omega_{ho}(m + 3/2) + \frac{1}{2}g \sum_{n_1 n_3} c(n_1, m, n_3, m) \hat{b}_{n_1}^\dagger \hat{b}_{n_3}. \quad (\text{A.11})$$

The average energy $\langle \hat{E}_m \rangle$ becomes, then,

$$\begin{aligned} \langle \hat{E}_m \rangle = \\ \hbar\omega_{ho}(m + 3/2) + \frac{1}{2}g \sum_{n_1 n_3} c(n_1, m, n_3, m) \langle \hat{b}_{n_1}^\dagger \hat{b}_{n_3} \rangle \delta_{n_1 n_3}, \end{aligned} \quad (\text{A.12})$$

which leads to Eq.(10).

In SFA, we define the energy operator by

$$\hat{E}_m = \langle \hat{E}_m \rangle + \Delta \hat{E}_m, \quad (\text{A.13})$$

where $\Delta \hat{E}_m$ is the fluctuation operator of the energy. The basic idea of SFA is to replace the square of the fluctuation operator with its mean value:

$$(\Delta \hat{E}_m)^2 \approx \langle (\Delta \hat{E}_m)^2 \rangle = \varphi_m^2. \quad (\text{A.14})$$

Going back to Eq.(A.6), one can write the solution to this equation as

$$\hat{b}_m^\dagger(\tau) = \hat{b}_m^\dagger(0) \exp[(\hat{E}_m)\tau] \exp(\Delta \hat{E}_m \tau). \quad (\text{A.15})$$

With the aid of the identity¹⁸,

$$B[a + b\Delta \hat{E}_m] \equiv \eta_0(m) + \eta_1(m) \Delta \hat{E}_m, \quad (\text{A.16})$$

where

$$\begin{aligned} \eta_0(m) &\equiv \frac{1}{2} \{B[a + b\varphi_m] + B[a - b\varphi_m]\}; \\ \eta_1(m) &\equiv \frac{1}{2\varphi_m} \{B[a + b\varphi_m] - B[a - b\varphi_m]\}; \end{aligned} \quad (\text{A.17})$$

we can rewrite Eq.(A.15) as follows:

$$\begin{aligned} \hat{b}_m^\dagger(\tau) = \\ \hat{b}_m^\dagger(0) \exp(\langle \hat{E}_m \rangle \tau) \left[\cosh(\varphi_m \tau) + \frac{\Delta \hat{E}_m}{\varphi_m} \sinh(\varphi_m \tau) \right]. \end{aligned} \quad (\text{A.18})$$

Using the identity

$$\langle \hat{A}(\beta) \hat{B} \rangle = \langle \hat{B} \hat{A} \rangle = \frac{1}{Q} \mathbf{Tr}[\exp(-\beta \hat{H}) \hat{B} \hat{A}], \quad (\text{A.19})$$

where Q is the Gibbs partition function, and replacing β with time τ , we can obtain the so-called long-range equation¹⁸

$$\langle \hat{n}_m \hat{A} \rangle = \eta_0(m) \langle \hat{A} \rangle + \eta_1(m) \langle \Delta \hat{E}_m \hat{A} \rangle, \quad (\text{A.20})$$

where, by invoking the chemical potential via $\hat{H} \rightarrow \hat{H} - \mu$,

$$\begin{aligned} \eta_0(m) &\equiv \frac{1}{2} \left\{ \frac{1}{\exp[\beta(\langle \hat{E}_m \rangle - \mu + \varphi_m)] - 1} + \frac{1}{\exp[\beta(\langle \hat{E}_m \rangle - \mu - \varphi_m)] - 1} \right\}; \\ \eta_1(m) &\equiv \frac{1}{2\varphi_m} \left\{ \frac{1}{\exp[\beta(\langle \hat{E}_m \rangle - \mu + \varphi_m)] - 1} - \frac{1}{\exp[\beta(\langle \hat{E}_m \rangle - \mu - \varphi_m)] - 1} \right\}. \end{aligned} \quad (\text{A.21})$$

The long-range equation is now applied to derive expressions for the fluctuations in the number of particles and the correlations between them. Substituting $\hat{A} = 1$ into this equation, and using the fact that the quadratic fluctuations are symmetric, i.e., $\langle \Delta \hat{E}_m \rangle = 0$, we obtain for the particle distribution

$$\langle \hat{n}_m \rangle = \eta_0(m). \quad (\text{A.22})$$

We also define the fluctuations in the number of particles $\Delta \hat{n}_m$ via

$$\Delta \hat{n}_m = \hat{n}_m - \langle \hat{n}_m \rangle, \quad (\text{A.23})$$

which then gives

$$\langle \Delta \hat{n}_m \hat{A} \rangle = \eta_1(m) \langle \Delta \hat{E}_m \hat{A} \rangle. \quad (\text{A.24})$$

Substituting $\hat{A} = \Delta \hat{n}_k$ into the long-range equation, we arrive at the expression

$$\langle \Delta \hat{n}_m \Delta \hat{n}_k \rangle_c = \eta_1(m) \langle \Delta \hat{E}_m \Delta \hat{n}_k \rangle, \quad (\text{A.25})$$

where the index c denotes true correlations, i.e., $m \neq k$.

Now the fluctuations in the energy arise from the interactions between the particles. It is straightforward to show that

$$\Delta \hat{E}_m = \frac{1}{2}g \sum_p c(p, m) \Delta \hat{n}_p. \quad (\text{A.26})$$

The true correlations between the fluctuations can be decomposed into

$$\langle \Delta \hat{n}_p \Delta \hat{n}_k \rangle = \langle (\Delta \hat{n}_k)^2 \rangle \delta_{p,k} + \langle \Delta \hat{n}_p \Delta \hat{n}_k \rangle_c. \quad (\text{A.27})$$

To find $\langle (\Delta \hat{n}_k)^2 \rangle$, we invoke Eq.(A.19) with $\hat{A} = \hat{b}_k^\dagger$ to get

$$\langle \hat{b}_k^\dagger(\beta) \hat{b}_k \hat{n}_k \rangle = \langle \hat{b}_k \hat{n}_k \hat{b}_k^\dagger \rangle. \quad (\text{A.28})$$

Applying the commutation relation $[\hat{n}_k, \hat{b}_k^\dagger] = \hat{b}_k$, we find that

$$\langle \hat{b}_k^\dagger(\beta) \hat{b}_k \hat{n}_k \rangle = \langle 1 + \hat{n}_k^2 + 2\hat{n}_k \rangle. \quad (\text{A.29})$$

Since the energy operator \hat{E}_m commutes with \hat{b}_k^\dagger and \hat{b}_k , Eq.(A.28) can be written in the form

$$\langle \hat{b}_k^\dagger(\beta) \hat{b}_k \hat{n}_k \rangle = \langle \exp[\beta(\hat{E}_k - \mu)] \hat{b}_k^\dagger \hat{b}_k \hat{n}_k \rangle. \quad (\text{A.30})$$

Setting $\hat{b}_k^\dagger \hat{b}_k = \hat{n}_k$ on the right side of (A.30), and equating it to the right side of (A.29), we get

$$\begin{aligned} \langle \hat{n}_k^2 \rangle &= \frac{1 + 2\hat{n}_k}{\exp[\beta(\hat{E}_k - \mu)] - 1} \\ &= \langle \hat{n}_k \rangle (1 + 2\langle \hat{n}_k \rangle) - 2\eta_1(k) \langle \hat{n}_k \Delta \hat{E}_k \rangle. \end{aligned} \quad (\text{A.31})$$

From Eq.(A.31) one can determine the fluctuations in the number of particles:

$$\begin{aligned} \langle (\Delta \hat{n}_k)^2 \rangle &= \langle \hat{n}_k^2 \rangle - \langle \hat{n}_k \rangle^2 \\ \langle (\Delta \hat{n}_k)^2 \rangle &= \langle \hat{n}_k \rangle (1 + \langle \hat{n}_k \rangle) + 2\eta_1(k) \frac{1}{2} g \sum_p c(k,p) \langle \Delta \hat{n}_p \Delta \hat{n}_k \rangle_c. \end{aligned} \quad (\text{A.32})$$

Setting $\hat{A} = \Delta \hat{E}$ in Eq.(A.24), we obtain an expression for the fluctuations in the energy, φ_m :

$$\eta_1(m) \varphi_m^2 = \langle \Delta \hat{n}_m \Delta \hat{E}_m \rangle = \sum_k c(k,m) \langle \Delta \hat{n}_m \Delta \hat{n}_k \rangle_c. \quad (\text{A.33})$$

Next, the Gibbs partition function is derived which contains the fluctuations. This is given by

$$\begin{aligned} Q &= \text{Tr}\{\exp[-\beta(\hat{H} - \hat{N}\mu)]\} = \\ &= \sum_{n_p} \exp\left[-\beta \sum_p (\hat{E}_p - \mu) \hat{n}_p\right] \\ &= \prod_p \sum_{n_p} \exp\left[-\beta (\hat{E}_p - \mu) \hat{n}_p\right]. \end{aligned} \quad (\text{A.34})$$

where $\hat{N} = \sum_p \hat{N}_p$. Taking the logarithm for convenience, we get

$$\begin{aligned}
 \ln Q &= \ln \left\{ \prod_p \sum_{n_p} \exp \left[-\beta (\hat{E}_p - \mu) \hat{n}_p \right] \right\} \\
 &= \sum_p \ln \left\{ \sum_{n_p} \exp \left[-\beta (\hat{E}_p - \mu) \hat{n}_p \right] \right\} \\
 &= \sum_p \ln \left\{ \frac{1}{1 - \exp \left[-\beta (\hat{E}_p - \mu) \right]} \right\}.
 \end{aligned} \tag{A.35}$$

Substituting $\hat{E}_m = \langle \hat{E}_m \rangle + \Delta \hat{E}_m$, and using the identity (A.16), we arrive at

$$\ln Q = - \sum_p \left[q_0(p, T) + q_1(p, T) \Delta \hat{E}_p \right]. \tag{A.36}$$

Considering the symmetry of the two eigenvalues of the energy fluctuation operator, we finally get

$$\begin{aligned}
 \ln Q &= - \sum_p q_0(p, T) \\
 q_0(p) &= \frac{1}{2} \ln \left(\left\{ 1 - \exp \left[-\beta (\langle \hat{E}_p \rangle - \mu + \varphi_p) \right] \right\} \times \right. \\
 &\quad \left. \left\{ 1 - \exp \left[-\beta (\langle \hat{E}_p \rangle - \mu - \varphi_p) \right] \right\} \right).
 \end{aligned} \tag{A.37}$$

From $q_0(p, T)$ all other thermodynamic properties follow.

A.3. $\ln Q$ in the limit $M \rightarrow \infty$

Assuming, then, that $\phi_F(m, T) \rightarrow 0$, we write first

$$\ln Q \approx - \sum_{m=0}^M \ln \left\{ 1 - \exp \left[-\beta (\hat{E}_m(T) - \mu(T)) \right] \right\}. \tag{A.38}$$

Following Grether *et al.*⁶, we evaluate the above sum by letting $M \rightarrow \infty$ and using their Eq.(6):

$$\Omega(T, V, \mu) = \Omega_0 - \frac{1}{\beta(\hbar\omega)^3} \sum_{\ell=1}^{\infty} \frac{[\exp(\beta(\mu(T) - 3\hbar\omega/2))]^\ell}{\ell^4}, \tag{A.39}$$

where

$$\Omega_0 = k_B T \ln \{ 1 - \exp[-\beta(3\hbar\omega/2 - \mu)] \} \tag{A.40}$$

is the ground-state contribution to the grand potential. Here we have used BE statistics and harmonic trapping in 3D. Using their Eq.(7), we obtain

$$\Omega(T, V, \mu) \equiv \Omega_0 - \frac{1}{\beta^4 (\hbar\omega)^3 \Gamma(4)} \int_0^\infty \frac{x^3}{z^{-1} \exp(x) - 1} dx. \quad (\text{A.41})$$

This can further be written

$$\Omega(T, V, \mu) = \Omega_0 - k_B T \left(\frac{k_B T}{\hbar\omega} \right)^3 g_4(\alpha), \quad (\text{A.42})$$

with $\alpha \equiv (\mu - 3\hbar\omega/2)/(k_B T)$. Apart from the fact that the treatment of Grether *et al.*⁶ uses a reference potential Ω_0 and a reference chemical potential $3\hbar\omega/2$, this thermodynamic potential is the same as Eq.(1) in the paper of Rochin²⁸ where the ‘harmonic’ pressure is also given by $P = -\Omega/V$, with $V = \omega^{-3}$ –the ‘harmonic’ volume.

In conclusion, then, Eq.(5) in our treatment with $\phi_F(m, T) \rightarrow 0$ and $M \rightarrow \infty$ gives the thermodynamic potential for a non-uniform trapped Bose gas. Hence all the thermal properties that follow from it are also suited for non-uniform systems. But as stated before, we were only able to use $M = 100$ because of our computational limitations.

1. M. Holzmann and J.-N. Fuchs and G. A. Baym and J.-P. Blaizot and F. Laloë, *C. R. Physique* **5**, p. 21 (2004).
2. J. G. Kim and E. K. Lee, *J. Phys. B: At. Mol. Opt. Phys.* **32**, p. 5575 (1999).
3. M. Li, H. Fu, Z. Zhang and J. Chen, *Phys. Rev. A* **75**, p. 045602 (2007).
4. S. Grossmann and M. Holthaus, *Phys. Lett. A* **208**, p. 188 (1995).
5. P. Öhberg and S. Stenholm, *J. Phys. B: At. Mol. Opt. Phys.* **30**, p. 2749 (1997).
6. M. Grether, M. Fortes, M. de Llano, J. L. del Río, F. J. Sevilla, M. A. Solís, and A. A. Valladares, *Eur. Phys. J. D* **23**, p. 117 (2003).
7. M. H. Anderson, J. R. Ensher, M. R. Matthews, C. E. Wieman and E. A. Cornell, *Science* **269**, p. 198 (1995).
8. S. J. Liu, G. X. Huang, L. Ma, S. Zhu and H. W. Xiong, *J. Phys. B: At. Mol. Opt. Phys.* **33**, p. 3911 (2000).
9. W. Ketterle and N. J. van Druten, *Phys. Rev. A* **54**, p. 656 (1996).
10. A. M. Kamchatnov, *Sov. Phys. JETP* **98**, p. 908 (2004).
11. S. Giorgini, L. P. Pitaevskii and S. Stringari, *Phys. Rev. A* **54**, p. R4633 (1996).
12. Y.-M. Kao and T. F. Jiang, *Phys. Rev. A* **73**, p. 043604 (2006).
13. Y.-M. Kao, D. H. Lin, P. Han and P.-G. Luan, *Eur. Phys. J. B* **34**, p. 55 (2003).
14. V. R. Rochin and V. S. Bagnato, *Braz. J. Phys.* **35**, p. 607 (2005).
15. R. Napolitano, J. D. Luca, V. S. Bagnato and G. C. Marques, *Phys. Rev. A* **55**, p. 3954 (1997).
16. G. Gnanapragasam, S.-H. Kim and M. P. Das, *Mod. Phys. Lett. B* **20**, p. 1839 (2006).
17. S. Giorgini, *Phys. Rev. A* **61**, p. 063615 (2000).
18. B. R. Joudeh, M. K. Al-Sugheir and H. B. Ghassib, *Int. J. Mod. Phys. B* **19**, p. 3985 (2005).
19. A. S. Sandouqa, M. K. Al-Sugheir and H. B. Ghassib, *Int. J. Theor. Phys.* **45**, p. 152 (2006).
20. R. R. Nigmatullin, A. A. Khamzin, and H. B. Ghassib, *Phys. Rev. E* **61**, p. 3441 (2000).

21. M. K. Al-Sugheir, H. B. Ghassib and R. R. Nigmatulin, *Int. J. Theor. Phys.* **40**, p. 1033 (2001).
22. M. K. Al-Sugheir and H. B. Ghassib, *Int. J. Theor. Phys.* **41**, p. 705 (2002).
23. N. M. Ghulam, H. B. Ghassib and M. K. Al-Sugheir, *Phys. Rev. C* **75**, p. 064317 (2007).
24. S. Sevincli and B. Tanatar, *Phys. Lett. A* **371**, p. 389 (2007).
25. V. I. Yukalov, *Phys. Rev. A* **72**, p. 033608 (2005).
26. W. H. Press, S. A. Teukolsky, W. T. Vetterling and B. B. Flannery, *Numerical Recipes in C*, second edn. (Cambridge University Press, 1999).
27. G. B. Arfken and H. J. Weber, *Mathematical Methods for Physicists*, fourth edn. (Academic Press, San Diego, USA, 1995).
28. V. R. Rochin, *Phys. Rev. Lett.* **94**, p. 130601 (2005).
29. F. Dalfovo, S. Giorgini, L. P. Pitaevskii and S. Stringari, *Rev. Mod. Phys.* **71**, p. 463 (1999).
30. G. Su, J. Chen and L. Chen, *Physica A* **368**, p. 459 (2006).
31. C. J. Pethick and H. Smith, *Bose-Einstein Condensation in Dilute Gases*, first edn. (Cambridge University Press, Cambridge UK, 2002).